Supplementary Information to

The Crystal Structure of Hexaphenylbenzene under High Hydrostatic Pressure

Gemma F. Turner,[1] Nicholas Stapleton,[1] James Brookes,[1] Dino Spagnoli,[1] Alif N. Sussardi,[2] Anita C. Jones,[2] Paul R. McGonigal,[3]* Stephen A. Moggach[1]*

[1] School of Molecular Sciences, The University of Western Australia, 35 Stirling Highway, Crawley, Perth, 6009, Western Australia, Australia

[2] School of Chemistry, The University of Edinburgh, Edinburgh, EH9 3FJ, United Kingdom

[3] Department of Chemistry, University of York, Heslington, York, YO10 5DD, North Yorkshire, United Kingdom

Contents

S1. Single Crystal X-Ray Diffraction

S1.1. Ambient Conditions

A colourless, platelet single crystal of C_6Ph_6 was characterised under ambient conditions by single crystal X-ray diffraction using a Rigaku Oxford Diffraction XtaLAB Synergy-S diffractometer,[1] equipped mirror-monochromated Mo Kα radiation (λ = 0.7107 Å) and a Hypix-6000HE detector. Diffraction data were integrated and corrected for absorption effects in CrysAlis Pro.[2] The crystal structure was solved using ShelXT [3] and refined using ShelXL [4] in Olex2.[5] All geometric and thermal parameters were refined freely. Hydrogen atoms were placed geometrically and constrained to ride on their host carbon atoms. In all geometric calculations, all C–H bond lengths were normalised to 1.089 Å.

S1.2. High-Pressure

The crystal of C_6Ph_6 previously characterised under ambient conditions was loaded in a modified miniature Merrill-Bassett diamond anvil cell,[6] equipped with a 40° opening angle, 600 µm culet Boehlar-Almax diamond anvils, tungsten carbide backing seats,[7] and a pre-indented tungsten gasket. An inert oil, MiTeGen LVCO-5 Cryo Oil™ was used as the pressure-transmitting medium. A chip of ruby was placed in the sample chamber to serve as a pressure calibrant. The pressure within the sample chamber was measured using the ruby fluorescence method.[8]

Diffraction data were collected on a Rigaku Oxford Diffraction XtaLAB Synergy-S diffractometer,[1] using Mo Kα radiation (λ = 0.7107 Å) up to 4.14 GPa. The crystal became amorphous by 4.45 GPa. The data collection strategy was determined by a high-pressure pre-experiment (using φ scans from -10 – 10° and 170 – 190°) in CrysAlis Pro.[2] Reflections from the diamond anvils and ruby chip were manually removed from sample reflections. Diffraction data were integrated and correction for absorption effects in CrysAlis Pro.[2]

The first high-pressure crystal structure at 0.22 GPa was refined against the starting coordinates of the structure model under ambient conditions. Subsequent high-pressure structures were refined using the starting coordinates of the model determined at the previous pressure. Crystal structures were refined using ShelXL[4] in Olex2.[5] Bonds lengths and 1,3-distances between the benzene core and the phenyl substituents were restrained to those in the structure under ambient conditions. The benzene core and each phenyl substituent were constrained to hexagonal geometry and were restrained to planarity. Incompleteness of the diffraction data caused by shading of the detector by the pressure cell precluded the refinement of anisotropic displacement parameters, and so all atoms were refined isotropically. Thermal similarity restraints were applied to each phenyl and benzyl ring. All torsional angles were allowed to refine freely. H-atoms were placed geometrically and constrained to ride on their host C-atom. In all geometric calculations, all C–H bond lengths were normalised to 1.089 Å.

Table S1. Abridged crystallographic data for C_6Ph_6 under variable applied pressure at T = 298 K. All data were collected on the same crystal using a Rigaku Synergy-S diffractometer with Mo Kα radiation (λ = 0.7107 Å).

	Ambient	**0.22 GPa**	**0.57 GPa**	**1.05 GPa**	**1.74 GPa**	**2.32 GPa**
Formula	$C_{42}H_{30}$	$C_{42}H_{30}$	$C_{42}H_{30}$	$C_{42}H_{30}$	$C_{42}H_{30}$	$C_{42}H_{30}$
M_r	534.66	534.66	534.66	534.66	534.66	534.66
Space group	$Pna2_1$	$Pna2_1$	$Pna2_1$	$P2_1/c$	$P2_1/c$	$P2_1/c$
a, *b*, *c* (Å)	12.1820(4), 11.7900(4), 20.8728(8)	12.1790(17), 11.8019(17), 20.61(3)	11.9478(13), 11.6849(13), 19.94(2)	11.4952(15), 19.71(3), 11.7143(18)	11.4968(17), 19.231(3), 11.6579(12)	11.4453(14), 18.97(2), 11.5585(17)
β (°)	90	90	90	91.020(13)	91.196(11)	91.276(13)
V (Å^3)	2997.87(18)	2963(4)	2783(3)	2653(3)	2576.9(6)	2510(3)
Z, *Z′*	4, 1	4, 1	4, 1	4, 1	4, 1	4, 1
Crystal size	0.26 x 0.17 x 0.03	0.26 x 0.17 x 0.03	0.26 x 0.17 x 0.03	0.26 x 0.17 x 0.03	0.26 x 0.17 x 0.03	0.26 x 0.17 x 0.03
Radiation	Mo Kα	Mo Kα	Mo Kα	Mo Kα	Mo Kα	Mo Kα
Diffractometer	Rigaku Synergy-S	Rigaku Synergy-S	Rigaku Synergy-S	Rigaku Synergy-S	Rigaku Synergy-S	Rigaku Synergy-S
Absorption correction	Multi-scan	Multi-scan	Multi-scan	Multi-scan	Multi-scan	Multi-scan
T_{min}, T_{max}	0.748, 1.000	0.329, 1.000	0.518, 1.000	0.394, 1.000	0.643, 1.000	0.074, 1.000
Measured, independent and observed reflns.	22696, 4282, 3478	6996, 1183, 789	6454, 958, 753	6773, 906, 529	4978, 909, 597	4489, 868, 526
R_{int}	0.044	0.119	0.088	0.210	0.098	0.117
$θ_{max}$ (°)	23.3	19.8	18.8	18.9	18.9	18.9
$(\sin θ/λ)_{max}$ (Å^{-1})	0.555	0.476	0.454	0.456	0.456	0.456
R_1, $ωR$, S	0.041, 0.102, 1.05	0.116, 0.366, 1.36	0.111, 0.364, 1.55	0.124, 0.369, 1.26	0.115, 0.369, 1.38	0.121, 0.349, 1.25
No. of reflections	4282	1183	958	906	909	868
No. of parameters	379	85	85	98	98	97
No. of restraints	1	53	95	111	81	81
H-atom treatment	Parameters constrained	Parameters constrained	Parameters constrained	Parameters constrained	Parameters constrained	Parameters constrained
$Δρ_{max}$, $Δρ_{min}$ (e Å^{-3})	0.11, -0.12	0.24, -0.23	0.34, -0.24	0.26, -0.28	0.33, -0.30	0.30, -0.28

S2. Bulk Modulus Calculation

The unit cell volume of C_6Ph_6 during hydrostatic compression was fitted to a second-order Birch-Murnaghan equation of state in the EoSFit7 program.[9] A second-order Birch-Murnaghan equation of state is given by *Equation 1*, where P is the applied pressure, K_0 is the isothermal bulk modulus, V_0 is the unit cell at ambient pressure and K'_{T_0} is the pressure derivative of the isothermal bulk modulus at standard temperature. The values of V_0 were set to the measured values.

$$P = \frac{3K_0}{2}\left[\left(\frac{V}{V_0}\right)^{\frac{7}{3}} - \left(\frac{V}{V_0}\right)^{\frac{5}{3}}\right] \quad (1)$$

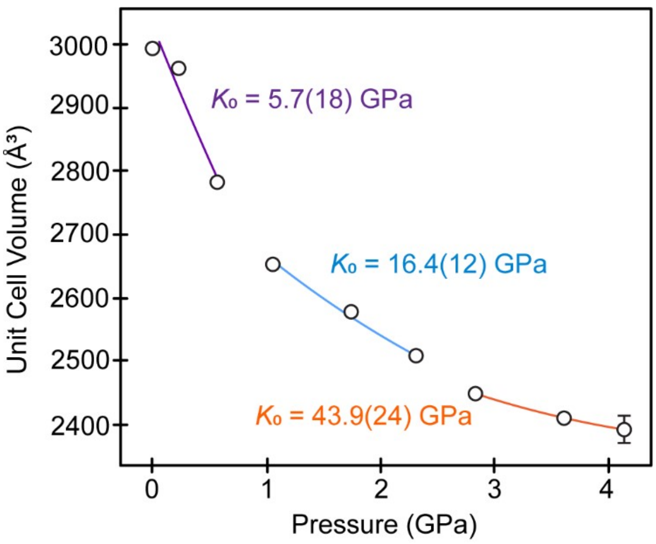

Figure S1. Third-order Birch-Murnaghan equation of state fits for C_6Ph_6 for the *Pna*2$_1$ phase (0.00 – 0.57 GPa, purple), single-crystalline of the *P*2$_1$/*c* phase (1.05 – 2.32 GPa, blue), and after the onset of amorphisation/degradation in crystallinity of the *P*2$_1$/*c* phase (2.82 – 4.14 GPa, orange).

S3. Intermolecular Interaction Energy Calculations in Crystal Explorer

Pairwise intermolecular interactions energies were calculated in Crystal Explorer (version 17).[10, 11] The crystal structure of C_6Ph_6 at ambient pressure and at each high-pressure point were used to determine the electron density matrix using Tonto, to a CE-B3LYP level of theory. Pairwise interactions were calculated between a central molecule and its neighbours in a cluster with a radius of ~12 Å.

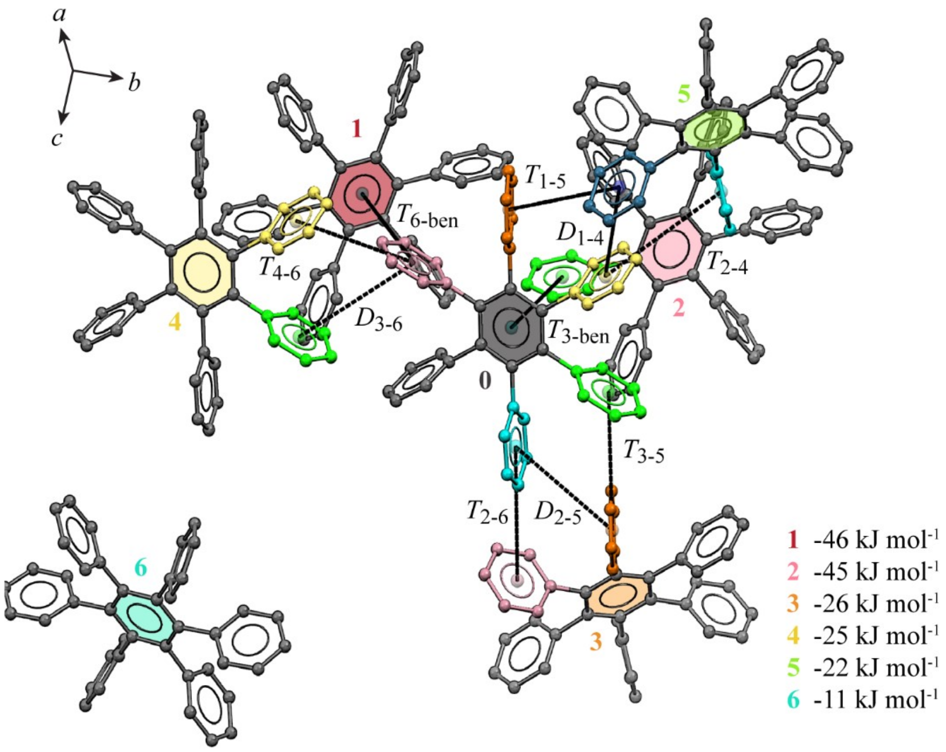

Figure S2. Cluster of C_6Ph_6 molecules showing the six most significant pairwise interactions and associated intermolecular phenyl dimers under ambient conditions of temperature and pressure.

Table S2. Pairwise interaction energies in C_6Ph_6 under ambient conditions. Energies are given in units of kJ mol^{-1}.

	1	**2**	**3**	**4**	**5**	**6**
R **(Å)** [a]	8.40	8.56	11.99	11.79	11.99	11.88
E_{disp}	-63.3	-58.2	-40.6	-31.2	-27.7	-14.7
E_{rep}	+34.6	+27.2	+31.0	+15.1	+12.7	+5.5
E_{elec}	-10.9	-9.5	-7.6	-5.5	-4.6	-1.5
E_{pol}	-0.9	-0.9	-2.1	-1.4	-1.4	-0.2
E_{tot}	-45.6	-44.6	-25.8	-24.7	-22.2	-11.2

[a] Distance between molecular centroids.

Table S3. Pairwise interaction energies in C_6Ph_6 at 0.22 GPa. Energies are given in units of kJ mol^{-1}.

	1	**2**	**3**	**4**	**5**	**6**
R **(Å)** [a]	8.40	8.56	11.8	11.8	11.88	11.76
E_{disp}	-66.3	-61.2	-42.6	-33.0	-29.0	-15.9
E_{rep}	+38.7	+31.4	+36.8	+18.8	+14.3	+7.2
E_{elec}	-12.9	-11.6	-9.0	-6.9	-5.0	-1.9
E_{pol}	-1.2	-1.2	-2.7	-1.8	-1.8	-0.3
E_{tot}	-48.4	-47.1	-25.9	-25.8	-23.1	-11.6

[a] Distance between molecular centroids.

Table S4. Pairwise interaction energies in C_6Ph_6 at 0.57 GPa. Energies are given in units of kJ mol^{-1}.

	1	**2**	**3**	**4**	**5**	**6**
R **(Å)** [a]	8.28	8.43	11.56	11.68	11.56	11.46
E_{disp}	-78.7	-73.4	-38.0	-37.8	-52.9	-19.6
E_{rep}	+58.2	+49.4	+27.2	+26.1	+60.2	+11.4
E_{elec}	-19.2	-16.9	-7.9	-8.6	-14.5	-2.7
E_{pol}	-1.6	-1.5	-2.5	-2.2	-4.3	-0.4
E_{tot}	-54.1	-52.4	-26.5	-27.5	-26.8	-13.1

[a] Distance between molecular centroids.

Table S5. Pairwise interaction energies in C_6Ph_6 at 1.05 GPa. Energies are given in units of kJ mol^{-1}.

	1	2	3	4	5	6
R **(Å)** [a]	8.13	8.28	11.41	11.50	11.41	11.46
E_{disp}	-94.1	-84.5	-60.9	-44.5	-46.0	-17.3
E_{rep}	+78.8	+76.5	+78.9	+38.0	+43.6	+9.0
E_{elec}	-25.2	-22.5	-18.3	-11.5	-11.5	-3.2
E_{pol}	-1.8	-1.9	-3.6	-2.3	-2.8	-0.3
E_{tot}	-61.3	-51.5	-26.4	-27.5	-27.4	-13.2

[a] Distance between molecular centroids.

Table S6. Pairwise interaction energies in C_6Ph_6 at 1.74 GPa. Energies are given in units of kJ mol^{-1}.

	1	2	3	4	5	6
R **(Å)** [a]	8.10	8.27	11.72	11.50	11.20	11.24
E_{disp}	-100.0	-90.6	-67.3	-47.3	-51.8	-19.5
E_{rep}	+92.4	+90.8	+99.7	+46.2	+54.5	+12.3
E_{elec}	-30.3	-27.3	-23.8	-14.2	-14.6	-4.2
E_{pol}	-2.2	-2.3	-4.3	-2.7	-3.3	-0.4
E_{tot}	-63.6	-53.3	-25.4	-29.6	-29.4	-14.2

[a] Distance between molecular centroids.

Table S7. Pairwise interaction energies in C_6Ph_6 at 2.32 GPa. Energies are given in units of kJ mol^{-1}.

	1	2	3	4	5	6
R **(Å)** [a]	8.04	8.22	11.08	11.50	11.08	11.11
E_{disp}	-107.8	-94.1	-73.3	-47.3	-57.7	-21.1
E_{rep}	+111.4	+104.0	+123.5	+46.2	+68.9	+15.1
E_{elec}	-35.9	-30.8	-29.9	-14.2	-18.2	-5.1
E_{pol}	-2.4	-2.4	-4.7	-2.7	-3.7	-0.5
E_{tot}	-64.8	-52.0	-22.7	-29.6	-29.7	-14.8

[a] Distance between molecular centroids.

S4. Intermolecular Phenyl Dimers Conformational Geometry

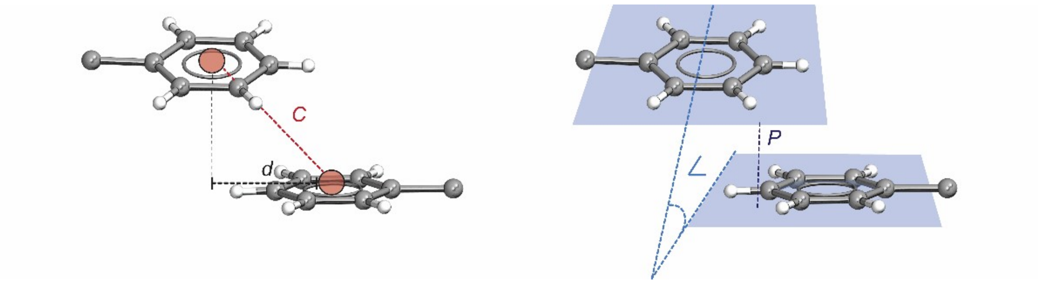

Figure S3. Conformational parameters for intermolecular phenyl dimers, values for which are given in the tables below.

All values of *C*, *P* and ∠ were measured in Mercury (Cambridge Structural Database) and corroborated in Olex2.

The displacement, *d*, was calculated by:

$$d = C \sin\left(\cos^{-1}\frac{P}{C}\right) \quad \text{(Equation S1)}$$

The absolute deviation of the conformational parameters from those in crystalline benzene were calculated by:

$$X = \left|(C - C_{benzene}) + (P - P_{benzene}) + (\angle - \angle_{benzene}) + (d - d_{benzene})\right| \quad \text{(Equation S2)}$$

Table S8. Conformational geometry of intermolecular, inter-layer phenyl dimer, $T_{6\text{-ben}}$.

P (GPa)	*C* (Å)	*P* (Å)	∠ (°)	*d* (Å)	*X*
0.000101325	5.176(4)	5.135(4)	81.64(6)	0.650(7)	14.86(1)
0.22	5.17(2)	5.13(2)	82.2(2)	0.626(3)	15.47(5)
0.57	5.04(2)	5.00(2)	80.5(2)	0.701(28)	13.34(4)
1.05	4.82(1)	4.80(1)	85.5(2)	0.404(20)	18.63(3)
1.74	4.76(1)	4.74(1)	85.0(2)	0.478(19)	18.06(3)
2.32	4.72(1)	4.70(1)	85.1(2)	0.504(20)	18.18(3)
Benzene T-shaped	5.01	4.92	75.40	0.90	0

Table S9. Conformational geometry of intermolecular, inter-layer phenyl dimer, $T_{3\text{-ben}}$.

P (GPa)	*C* (Å)	*P* (Å)	∠ (°)	*d* (Å)	*X*
0.000101325	5.076(4)	5.041(4)	74.190(4)	0.595(7)	9.687(10)
0.22	5.09(2)	5.06(2)	74.45(3)	0.58(3)	8.57(5)
0.57	4.96(2)	4.91(2)	77.54(2)	0.70(3)	10.36(4)
1.05	4.82(1)	4.80(1)	85.48(2)	0.40(2)	18.63(3)
1.74	4.76(1)	4.74(1)	84.99(2)	0.48(2)	18.06(3)
2.32	4.72(1)	4.70(1)	85.14(2)	0.504(2)	18.18(3)
Benzene T-shaped	5.01	4.92	75.40	0.90	0

Table S9. Conformational geometry of intermolecular, intra-layer phenyl dimer, $T_{1\text{-}5}$.

P (GPa)	*C* (Å)	*P* (Å)	∠ (°)	*d* (Å)	*X*
0.000101325	5.520(5)	4.411(5)	60.190(7)	3.319(9)	20.78(1)
0.22	5.49(2)	4.41(2)	60.81(3)	3.28(3)	20.16(5)
0.57	5.30(2)	4.34(2)	61.53(2)	3.04(3)	19.42(4)
1.05	4.94(1)	4.73(1)	70.14(2)	1.40(2)	12.63(3)
1.74	4.87(1)	4.70(1)	71.38(2)	1.26(6)	11.57(3)
2.32	4.78(1)	4.66(1)	72.15(2)	1.07(2)	11.04(3)
Benzene T-shaped	5.01	4.92	75.40	0.90	0

Table S10. Conformational geometry of intermolecular, intra-layer phenyl dimer, $T_{3\text{-}5}$.

P (GPa)	*C* (Å)	*P* (Å)	∠ (°)	*d* (Å)	*X*
0.000101325	5.712(5)	5.142(5)	63.270(7)	2.487(9)	19.45(1)
0.22	5.65(2)	5.14(2)	64.44(3)	2.34(4)	18.37(6)
0.57	5.42(2)	4.88(2)	62.04(3)	2.36(3)	20.26(5)
1.05	5.38(1)	4.91(1)	63.28(2)	2.21(2)	19.15(3)
1.74	5.24(1)	4.78(1)	63.25(3)	2.15(2)	19.00(3)
2.32	5.10(1)	4.64(1)	63.18(2)	2.10(2)	18.81(3)
Benzene T-shaped	5.01	4.92	75.40	0.90	0

Table S11. Conformational geometry of intermolecular, intra-layer phenyl dimer, $T_{4\text{-}6}$.

P (GPa)	*C* (Å)	*P* (Å)	∠(°)	*d* (Å)	*X*
0.000101325	5.408(4)	4.714(4)	61.300(6)	2.650(7)	19.53(1)
0.22	5.39(2)	4.62(2)	59.70(3)	2.77(4)	21.88(5)
0.57	5.26(2)	4.54(2)	59.08(3)	2.66(3)	22.42(5)
1.05	5.19(1)	4.41(1)	59.48(2)	2.74(2)	21.74(3)
1.74	5.17(1)	4.36(1)	57.37(2)	2.77(2)	23.75(3)
2.32	5.16(2)	4.41(1)	56.54(2)	2.67(2)	24.71(3)
Benzene T-shaped	5.01	4.92	75.40	0.90	0

Table S12. Conformational geometry of intermolecular, intra-layer phenyl dimer, $T_{2\text{-}4}$.

P (GPa)	*C* (Å)	*P* (Å)	∠(°)	*d* (Å)	*X*
0.000101325	5.135(5)	4.910(5)	67.870(7)	2.035(8)	14.68(1)
0.22	5.27(2)	4.86(2)	68.12(3)	2.04(3)	14.33(5)
0.57	5.12(2)	4.74(2)	68.63(3)	1.93(3)	13.66(5)
1.05	5.32(1)	4.03(1)	60.00(2)	3.47(2)	20.27(3)
1.74	5.22(1)	3.99(1)	61.67(2)	3.37(2)	18.52(3)
2.32	5.17(2)	3.94(1)	62.80(2)	3.35(2)	17.33(3)
Benzene T-shaped	5.01	4.92	75.40	0.90	0

Table S13. Conformational geometry of intermolecular, intra-layer phenyl dimer, $T_{2\text{-}6}$.

P (GPa)	*C* (Å)	*P* (Å)	∠(°)	*d* (Å)	*X*
0.000101325	5.700(5)	4.782(5)	49.830(7)	3.102(9)	31.91(1)
0.22	5.61(2)	4.79(2)	52.19(3)	2.91(4)	29.66(5)
0.57	5.33(2)	4.63(2)	52.39(3)	2.66(3)	29.27(5)
1.05	5.09(1)	4.42(1)	50.58(2)	2.54(2)	30.74(3)
1.74	4.95(1)	4.34(1)	51.44(2)	2.38(2)	30.00(3)
2.32	4.88(1)	4.38(1)	51.54(2)	2.26(2)	30.03(2)
Benzene T-shaped	5.01	4.92	75.40	0.90	0

Table S14. Conformational geometry of intermolecular, intra-layer phenyl dimer, $D_{1\text{-}4}$.

P (GPa)	***C* (Å)**	***P* (Å)**	**∠(°)**	***d* (Å)**	***X***
0.000101325	4.436(4)	3.378(4)	15.520(6)	2.875(7)	18.31(1)
0.22	4.39(2)	3.39(2)	16.23(3)	2.80(3)	19.06(5)
0.57	4.11(2)	3.25(2)	10.81(3)	2.52(3)	13.48(5)
1.05	3.96(2)	3.14(1)	9.00(2)	2.40(3)	11.54(3)
1.74	3.80(2)	3.11(1)	6.90(2)	2.18(2)	9.76(3)
2.32	3.68(1)	2.98(1)	6.37(2)	2.16(2)	9.25(3)
Benzene Displaced-stacked	3.95	3.54	0	1.74	0

Table S15. Conformational geometry of intermolecular, intra-layer phenyl dimer, $D_{2\text{-}5}$.

P (GPa)	***C* (Å)**	***P* (Å)**	**∠(°)**	***d* (Å)**	***X***
0.000101325	4.920(6)	2.960(6)	16.080(8)	3.93(1)	18.65(2)
0.22	4.89(2)	3.02(2)	15.09(3)	3.85(3)	17.61(5)
0.57	4.65(2)	2.99(2)	11.83(2)	3.56(3)	13.79(4)
1.05	4.46(1)	3.16(2)	13.56(2)	3.16(2)	15.86(3)
1.74	4.38(1)	2.913(1)	13.23(2)	3.27(2)	15.09(3)
2.32	4.27(1)	2.874(1)	13.93(2)	3.16(2)	15.57(3)
Benzene Displaced-stacked	3.95	3.54	0	1.74	0

Table S16. Conformational geometry of intermolecular, intra-layer phenyl dimer, $D_{3\text{-}6}$.

P (GPa)	***C* (Å)**	***P* (Å)**	**∠(°)**	***d* (Å)**	***X***
0.000101325	5.219(4)	3.054(4)	9.290(6)	4.232(8)	12.55(1)
0.22	5.20(2)	2.97(2)	8.50(2)	4.27(4)	11.70(6)
0.57	5.04(2)	3.09(2)	4.04(2)	3.99(4)	6.92(6)
1.05	4.84(1)	3.28(1)	0.00(2)	3.56(2)	2.45(3)
1.74	4.81(1)	3.1(1)	0.00(2)	3.66(2)	2.34(3)
2.32	4.73(1)	2.95(1)	0.00(2)	3.69(2)	2.13(2)
Benzene	3.95	3.54	0	1.74	0

Displaced-stacked

S6. Molecular Geometry

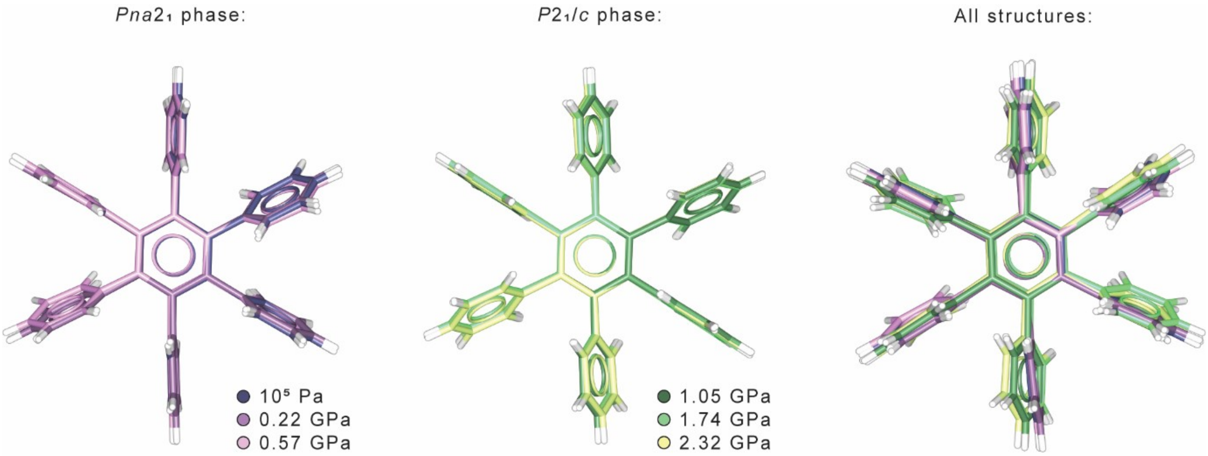

Figure S4. Overlay of the molecular structure of hexaphenylbenzene during hydrostatic compression between ambient pressure and 0.57 GPa (left, $Pna2_1$ phase, purple/pink), 1.05 GPa to 2.32 GPa (centre, $P2_1/c$ phase, green/yellow), at all pressures (right). There are no intramolecular interactions between phenyl groups. The largest change in torsional angle of the phenyl substituents during compression is 3° but the change is not statistically significant.

S7. Density Functional Theory

Once an ambient and high-pressure phase of hexaphenylbenzene had been structurally elucidated, both underwent computational modelling with periodic DFT methods, using the VASP software (version 6.3.2).[12-14] Geometry optimisations were carried out in a multistep process. Initially, the experimental structures were optimised with fixed unit cell parameters, then the resulting geometries were used as starting points for a second optimisation with unconstrained unit cell parameters, followed by a single energy point calculation. This process has been shown to improve periodic DFT optimisation convergence when beginning with experimental structural data of molecular crystals.[15] Pressure equal to the measured experimental value was simulated and applied to the high-pressure phase (1.05 GPa) during relevant optimisations. Gas-phase optimisations were performed with a unit cell large enough to ensure at least 14 Å of separation from adjacent periodic molecules. This methodology has been used in similar periodic DFT calculations by Moellmann and Grimme as a good approximation for isolated systems in plane-wave-based software.[16]

All calculations were performed with the PBE exchange-correlation functional,[17] using the state-of-the-art D4 dispersion correction from Caldeweyher *et al*.[18] This method was shown in later work to outperform the often-used PBE with Beck-Johnson damped D3 correction for recreating experimental unit cell volumes and lattice energies of molecular crystals.[19] A large plane-wave basis with a 1000 eV cutoff was used in all calculations, alongside projector-augmented wave (PAW) potentials with hard pseudopotentials.[20, 21] The convergence criteria was set to $1x10^{-7}$ eV for electronic structure and $1x10^{-3}$ eV $Å^{-1}$ for atomic movement.

The Brillouin zone was sampled with the tetrahedron method with Blöchl corrections and a Γ-centred grid generated with an automatic k-point mesh.[22] This gave rise to 2x3x1 and 3x2x3 *k*-points for the ambient and high-pressure unit cells, respectively. The value used to generate k-points, R_K, was found to be converged at R_K = 30. The gas phase calculation used a Monkhorst-Pack grid with 1x1x1 *k*-points.

To obtain the electronic density of states (DOS), single energy point calculations were performed on experimental structures of both phases with a higher density Γ-centred Monkhorst-Pack grid spanning 6x9x3 and 9x6x9 *k*-points for ambient and high-pressure structures, respectively. Band structure and band gap information was determined by single point energy calculations through high-symmetry k-paths obtained using the *SeeK-path* tool.[23, 24] Due to the exceeding computational cost associated with these calculations, the number of intersections per k-path was limited to 10. The absorbance properties of each phase were determined applying the VASP keyword "LOPTICS" to calculate the dielectric matrix, with a mesh of 4x6x2 and 6x4x6 for the ambient and high-pressure phases respectively. The DOS, band-structure and absorbance were plotted using the *sumo* command-line tools.[25]

The cohesion energy of the crystal was calculated using the below formula:

$$E_{coh} = \frac{E_{uc}}{N} - E_{gas}$$

Where N = number of molecules per unit cell (which in both cases N = 4), E_{coh} is the cohesion energy, E_{uc} is the total energy of the unit cell, and E_{gas} is the energy of the isolated gas phase molecule.

Table S17. Theoretical photophysical properties of hexaphenylbenzene at ambient pressure and 2.32 GPa from density functional theory.

P **(GPa)**	**Band gap (eV)**	**Absorption (nm) 1**	**Absorption (nm) 2**	**Absorption (nm) 3**
0.00	3.75	100	120	264
2.32	3.30	87.9	105	230

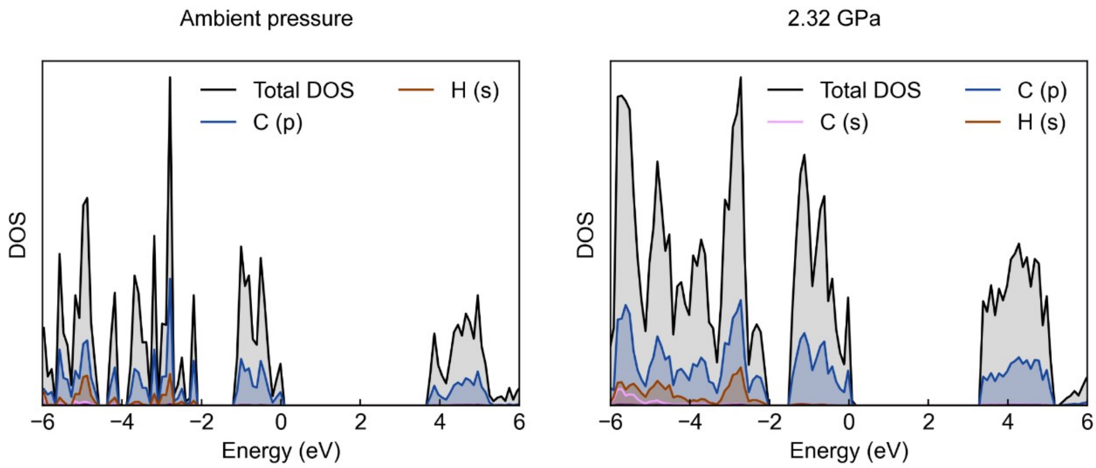

Figure S5. Density of states (DOS) plots of the ambient pressure *Pna*2$_1$ phase of hexaphenylbenzene (left) and high-pressure *P*2$_1$/*c* phase of hexaphenylbenzene (right).

References

1. P. Le Magueres, E. W. Reinheimer, M. Meyer, A. Jones and D. Kucharczyk, *Acta Crystallogr A Found Adv*, 2018, **A74**, 468.
2. C. P. R. O. Agilent and P. R. O. CrysAlis, *Yarnton, Oxfordshire, England*, 2014.
3. G. M. Sheldrick, *Acta Crystallogr A Found Adv*, 2015, **71**, 3-8.
4. G. M. Sheldrick, *Acta Crystallogr C Struct Chem*, 2015, **71**, 3-8.
5. O. V. Dolomanov, L. J. Bourhis, R. J. Gildea, J. A. K. Howard and H. Puschmann, *Journal of Applied Crystallography*, 2009, **42**, 339-341.
6. L. Merrill and W. A. Bassett, *Rev Sci Instrum*, 1974, **45**, 290-294.
7. S. A. Moggach, D. R. Allan, S. Parsons and J. E. Warren, *Journal of Applied Crystallography*, 2008, **41**, 249-251.
8. G. J. Piermarini, S. Block, J. D. Barnett and R. A. Forman, *Journal of Applied Physics*, 1975, **46**, 2774-2780.
9. J. Gonzalez-Platas, M. Alvaro, F. Nestola and R. Angel, *Journal of Applied Crystallography*, 2016, **49**, 1377-1382.
10. S. K. Wolff, D. J. Grimwood, J. J. McKinnon, M. J. Turner, D. Jayatilaka and M. A. Spackman, *Crystal Explorer*, 2012.
11. C. F. MacKenzie, P. R. Spackman, D. Jayatilaka and M. A. Spackman, *IUCrJ*, 2017, **4**, 575-587.
12. G. Kresse and J. Hafner, *Phys. Rev. B*, 1994, **49**, 14251-14269.
13. G. Kresse and J. Furthmüller, *Comput. Mater. Sci.*, 1996, **6**, 15-50.
14. G. Kresse and J. Furthmüller, *Phys. Rev. B*, 1996, **54**, 11169-11186.
15. J. van de Streek and M. A. Neumann, *Acta Cryst. B*, 2010, **B66**, 544-558.
16. J. Moellmann and S. Grimme, *J. Phys. Chem.*, 2014, **118**, 7615-7621.
17. J. P. Perdew, K. Burke and M. Ernzerhof, *Phys. Rev. Lett.*, 1996, **77**, 3865-3868.
18. E. Caldeweyher, S. Ehlert, A. Hansen, H. Neugebauer, S. Spicher, C. Bannwarth and S. Grimme, *J. Phys. Chem.*, 2019, **150**, 154122.
19. E. Caldeweyher, J.-M. Mewes, S. Ehlert and S. Grimme, *Phys. Chem. Chem. Phys.*, 2020, **22**, 8499-8512.
20. P. E. Blöchl, *Phys. Rev. B*, 1994, **50**, 17953-17979.
21. G. Kresse and D. Joubert, *Phys. Rev. B*, 1999, **59**, 1758-1775.
22. P. E. Blöchl, O. Jepsen and O. K. Anderson, *Phys. Rev. B*, 1994, **49**, 16223-16233.
23. Y. Hinuma, G. Pizzi, Y. Kumagai, F. Oba and I. Tanaka, *Comput. Mater. Sci.*, 2017, **128**.
24. A. Togo and I. Tanaka, *arXiv*, 2018.
25. A. M. Ganose, A. J. Jackson, O. Scanlon and D. Sumo, *J. Open Source Softw.*, 2018, **3**.